State-specific Peptide Design Targeting G Protein-coupled Receptors

Yang Xue*[1], Hong Wang*[2], Jun Li*[1], Jianguo Hu[2], Zhiyuan Chen[1], Zhi Zheng[2], Lihang Liu[1], Kunrui Zhu[1], Jingzhou He[1], Huanzhang Gong[2,✉], Xiangqun Li[2,✉], Xiaonan Zhang[1,✉], and Xiaomin Fang [1,✉]

[1]Baidu Inc.
[2]Zonsen PepLib Biotech Inc.

G protein-coupled receptors (GPCRs) play critical roles in various physiological processes and serve as pivotal targets for drug discovery. Peptides are particularly compelling therapeutic agents for targeting GPCRs, as they frequently exhibit superior affinity, selectivity, and potency compared to small-molecule drugs. However, the states (active and inactive) of GPCRs profoundly influence their interactions with ligands, highlighting the need for state-specific strategies in peptide design. To address this, we developed an efficient state-specific peptide design pipeline targeting GPCRs. This framework enables the tailored design of agonists or antagonists based on the active or inactive conformational states of GPCR structures. A state-specific folding model, optimized for GPCR-peptide complexes, was used to select high-potential peptides from the pool of designed candidates. Using this approach, we successfully identified both agonist and antagonist peptides for the Apelin Receptor (APJR) and the Growth Hormone Secretagogue Receptor (GHSR), as well as a competitive inhibitor for the Glucagon-Like Peptide-1 Receptor (GLP-1R).

Introduction

G-protein-coupled receptors (GPCRs) are a large and diverse group of membrane receptors that play crucial roles in cellular signal transduction. Their involvement in various physiological processes makes them attractive targets for therapeutic intervention (Santos et al., 2017). Despite the success of small molecules and biologics in modulating GPCR activity, these approaches often face limitations such as off-target effects (Weiss et al., 2018). Peptide-based therapeutics offer a promising alternative due to their remarkable pharmacodynamic properties: high affinity, selectivity and potency (Wang et al., 2022b; Davenport et al., 2020).

Conventional methods for developing peptide drugs involve leveraging natural peptides and hormones found in the human body, as well as creating peptides that mimic these hormones (Alavi et al., 2019; Wilson et al., 2007; Pokuri et al., 2016). Peptides can also be sourced from natural products, including those derived from bacteria, fungi, and plants (Brown et al., 2007; Yamazaki et al., 2009; Toivanen et al., 2017; Mygind et al., 2005; Matsubayashi and Sakagami, 2006). Another approach involves the use of phage display techniques to discover and optimize peptide candidates (Omidfar and Daneshpour, 2015).

Recently, AI-based peptide rational design has gathered increasing attention (Hill et al., 2014; Nevola and Giralt, 2015; Chang et al., 2022). EvoBind (Bryant and Elofsson, 2022; Li et al., 2024) employs in silico-directed evolution to design peptides and then evaluates the designs using confidence scores from the folding model AlphaFold-Multimer (Evans et al., 2021). EvoPlay (Wang et al., 2023) improves it by replacing directed evolution with Monte Carlo tree search (MCTS) and reinforcement learning policy (Silver et al., 2016), leading to more data-efficient peptide design. Additionally, PepMLM (Chen et al., 2023) uses a protein language model (PLM) to design peptide binders. Approaches for designing mini-proteins may also be applicable to peptide designs, such as AlphaFold-2 hallucination (Vázquez Torres et al., 2024), RFDiffusion-MPNN (Vázquez Torres et al., 2024), AlphaProteo (Zambaldi et al., 2024) and BindCraft (Pacesa et al., 2024).

*These authors contributed equally to this work
✉ Corresponding authors: gong_huanzhang@peplib.com (H. Gong), li_xiangqun@peplib.com (X. Li), zhangxiaonan@baidu.com (X. Zhang), fangxiaomin01@baidu.com (X. Fang)

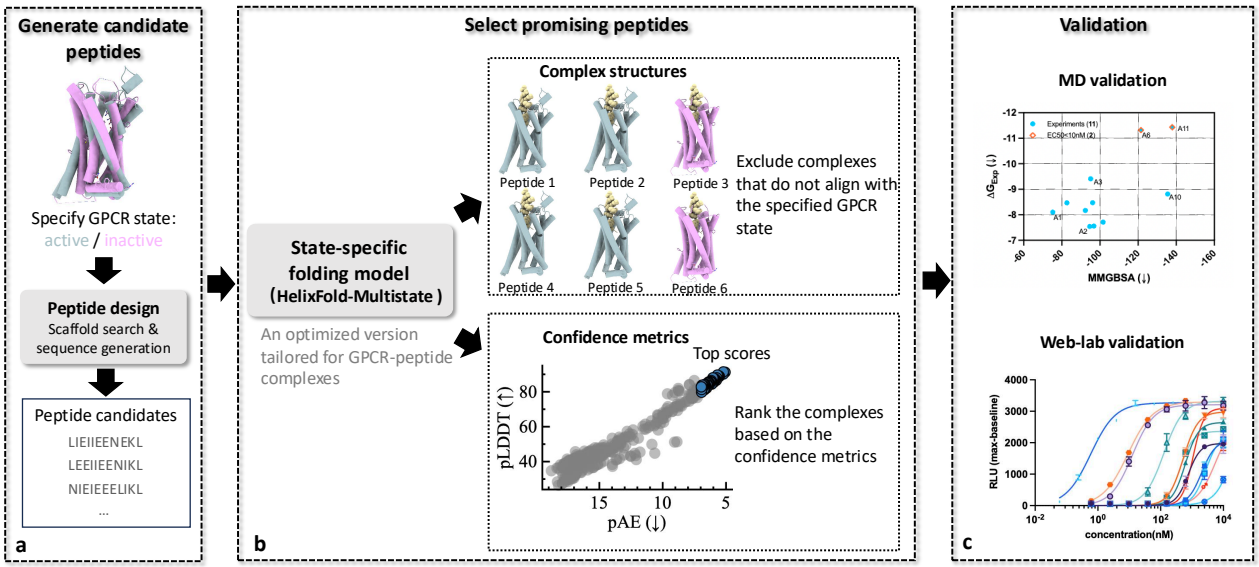

Figure 1. State-specific peptide design pipeline.
(a) Generation of the candidate peptides through the peptide design modules. **(b)** State-specific folding model (HelixFold-Multistate), an optimized version tailored for GPCR-peptide complexes, to select promising peptides. **(c)** In-silico molecular dynamic (MD) simulation and web-lab experimental validation.

Although AI-driven peptide design approaches have successfully generated high-affinity binders, targeting GPCRs presents unique challenges due to their dynamic conformational landscape and functional plasticity. GPCRs can adopt multiple active and inactive states, each stabilized by distinct ligand interactions, which determine whether a peptide functions as an agonist or antagonist. Effective GPCR-targeting peptides must not only achieve high binding affinity but also selectively stabilize specific receptor conformations, thereby modulating the energy landscape to favor desired functional outcomes. Therefore, integrating GPCR conformational states and state-specific interactions into peptide design strategies is critical for achieving precise modulation of receptor activity. Existing approaches for peptide design targeting GPCRs, such as HelixDiff (Xie et al., 2024), typically define the structure of the GPCR protein used in the generation model. However, these methods do not allow for precise control over the GPCR's functional state (e.g., active or inactive). This limitation hinders the ability to design peptide agonists and antagonists that accurately correspond to specific receptor states.

In this study, we present a computational method for state-specific peptide design targeting GPCRs (Figure 1). The workflow begins with the generation of a diverse pool of candidate peptides using a peptide design module (Hsu et al., 2022; Dauparas et al., 2022) (Figure 1a). A state-specified folding model (Figure 1b) is then employed to define the active or inactive states of GPCR targets, predict the structures of GPCR-peptide complexes, and assign a confidence score to each complex. Complexes that do not align with the specified GPCR state, such as those with the binding pocket located within the membrane or those exhibiting a significant RMSD in the state-specific TM domain compared to the expected state, are filtered out. The remaining complexes are then ranked based on the integrated application of multiple confidence metrics. This ranking process allows for the prioritization of peptide candidates with the highest likelihood of success for further validation through in silico and experimental methods (Figure 1c). To refine the folding model for GPCR-peptide interactions, we fine-tuned HelixFold-Multimer (HF-Multimer) (Fang et al., 2024), a reproduction of AlphaFold-Multimer (AF-Multimer) (Evans et al., 2021) on GPCR-peptide (Pándy-Szekeres et al., 2023) and protein-peptide (Martins et al., 2021) datasets. This refinement resulted in improved predictive accuracy for GPCR-peptide complexes. Furthermore, we incorporated state-specific modeling techniques inspired by AlphaFold-Multistate (AF-Multistate) (Heo and Feig, 2022), enabling precise differentiation between the active and inactive states of GPCRs. These advancements facilitate the rational design of peptide agonists and antagonists specifically tailored to target specific GPCR receptors. The resulting model, named HelixFold-Multistate (HF-Multistate), provides a robust computational tool for advancing the design of state-specific peptide therapeutics targeting GPCRs.

We validated that the GPCR-peptide structures predicted by HelixFold-Multistate are more effective at preserving the correct activation states of GPCRs while providing more accurate GPCR-peptide interaction poses for both active and inactive states of GPCR targets. Furthermore, the structural confidence scores derived from HelixFold-Multistate

demonstrated a strong correlation with experimental affinity data for both peptide agonists and antagonists. We tested the state-specific peptide design pipeline by designing both agonists and antagonists for three GPCR targets, Apelin Receptor (APJR) and Glucagon-Like Peptide-1 Receptor (GLP-1R), and Growth Hormone Secretagogue Receptor (GHSR) using in-silico and experimental validation. Designing antagonistic peptides for GPCRs is more challenging than agonists. The pipeline successfully identified high-affinity agonists (<100 nM) and moderate-affinity antagonists, highlighting the precision and flexibility of the proposed methodology. Notably, the agonist peptides targeting APJR exhibit a high affinity, with an EC50 < 10 nM. The antagonist peptides targeting GLP-1R have an IC50 of 874 nM.

Results

We first evaluated the structural prediction accuracy and screening effectiveness of the optimized state-specific folding model, HF-Multistate, which serves as the most critical component of our peptide design pipeline. Following this, we assessed the pipeline's performance by designing peptides for three GPCR targets, aiming to evaluate its ability to generate target-specific agonists and antagonists.

GPCR-Peptide Structure Prediction Capacity

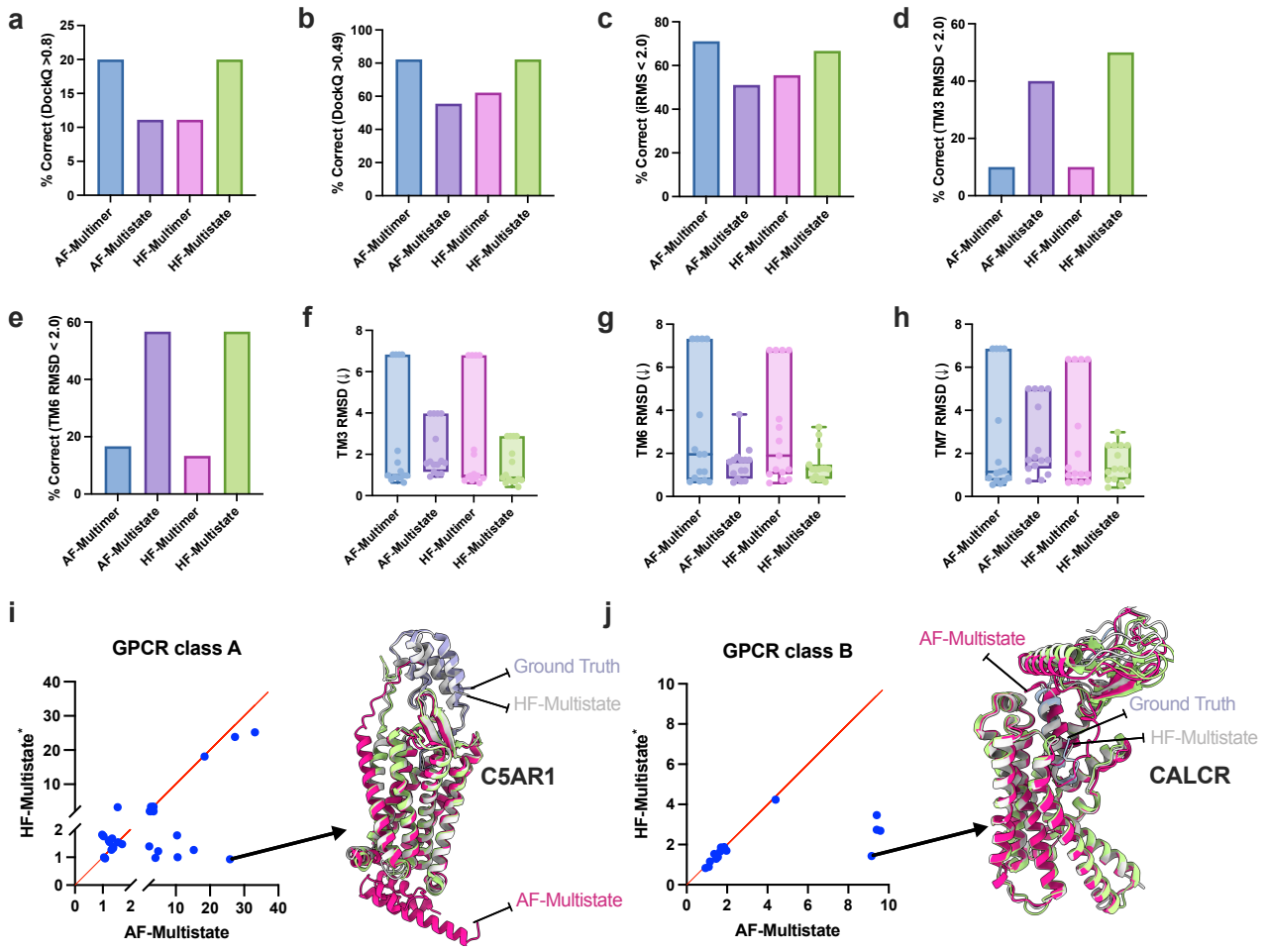

Figure 2. Comparison of folding models for structural prediction accuracy in recent GPCR-peptide complexes from the PDB.
(a-c) Comprehensive assessment of GPCR-peptide interface prediction accuracy using multiple evaluation metrics. **(d-e)** Assessment of structural accuracy in GPCR States through evaluation of the transmembrane (TM) domain in GPCR class A. **(f-h)** Assessment of the TM domain in GPCR class B. **(i-j)** Scatter plot comparison of iRMS between AF-Multistate and HF-Multistate for GPCR Class A and Class B families.

We evaluated the performance of different folding models from two perspectives: the accuracy of GPCR-peptide interface predictions and the structural accuracy of GPCR states, particularly in key regions. Our optimized state-specific folding model, HelixFold-Multistate (HF-Multistate), was benchmarked against AlphaFold-Multimer (AF-Multimer) (Evans et al., 2021), HelixFold-Multimer (HF-Multimer) (Fang et al., 2024) and AlphaFold-Multistate (AF-Multistate) (Evans et al., 2021). It is worth noting that AF-Multimer and AF-Multistate utilize an ensemble of five models, each executed five times with different random seeds for each prediction. In contrast, HF-Multimer and HF-Multistate achieve competitive results using a single model executed five times with varying seeds.

We employed multiple evaluation metrics, including DockQ (Basu and Wallner, 2016), interface root-mean-square deviation (iRMS, a component of DockQ), % Correct (DockQ > 0.8), % Correct (DockQ > 0.49), and % Correct (iRMS < 2.0), to comprehensively assess the performance of various folding models in predicting GPCR-peptide interfaces. As shown in Figure 2(a-c), HF-Multistate exhibits performance on par with AF-Multimer and outperforms AF-Multistate and HF-Multimer. While AF-Multistate has been demonstrated to accurately predict the activation states of monomeric GPCRs (Heo and Feig, 2022), it faces limitations in predicting interactions within GPCR-peptide complexes. The comparison between HF-Multistate and AF-Multistate highlights the importance of incorporating GPCR-peptide complex structural data for fine-tuning, as such data can improve predictive accuracy, particularly in modeling state-specific interactions.

Standard evaluation metrics, such as DockQ, are often insufficiently sensitive to structural precision in critical regions, including the transmembrane (TM) domain (Heo and Feig, 2022), which is fundamental to GPCR function and signaling. To address this limitation, we conducted a focused analysis of TM domain structural accuracy across two major GPCR families: Class A (rhodopsin-like receptors) and Class B (secretin-like receptors). Following the methodology outlined in a previous study (Hauser et al., 2021), we focused our analysis on TM3 and TM6 for Class A GPCRs, on TM3, TM6, and TM7 for Class B GPCRs, since these regions are crucial for peptide hormone recognition and receptor activation. In Class A GPCRs, TM3 and TM6 undergo state-dependent conformational changes: TM6 moves outward in active states to facilitate G-protein binding. At the same time, TM3 exhibits a cytosolic tilt and overall rotation with only minor changes. In Class B GPCRs, TM3, TM6, and TM7 exhibit more intricate state-specific dynamics: TM6 undergoes outward shifts to drive receptor activation, TM3 maintains structural integrity through minor adjustments, and TM7's extracelluar region undergoes significant conformational changes to enable peptide hormone binding and activation. Across both classes, TM3 and TM6 function as key 'macroswitches' in the receptor activation process. Figures 2(d-e) and (f-h) present a comparative analysis of the performance of multiple folding models on TM domains for Class A and Class B GPCRs, respectively. For Class B GPCRs, the comparison of % Correct (TM RMSD < 2.0) is not very significant. Therefore, we included the distribution of all data points for clarity. AF-Multistate and HF-Multistate outperform AF-Multimer in structural prediction accuracy across the TM domains, with notable improvements in the critical TM3 and TM6, emphasizing the advantages of state-specific modeling. More importantly, HF-Multistate consistently achieves the highest precision across all key TM domains in terms of TM RMSD, highlighting HF-Multistate's superior ability to incorporate the distinct activation states of GPCRs during peptide binding, providing a deeper understanding of their functional dynamics.

To provide a more detailed comparison, we analyzed two representative cases: C5AR1 and CALCR. For C5AR1 in Figure 2i, HF-Multistate accurately predicts the G-protein binding pocket, whereas AF-Multistate erroneously identifies an incorrect pocket. For CALCR in Figure 2j, while AF-Multistate identifies the correct binding pocket, it misorients the peptide, causing the N-terminus to face upward, a mistake not observed with HF-Multistate. These findings highlight the inherent challenges in predicting GPCR-peptide complex structures and underscore the importance of refining models with relevant structural data to achieve improved predictive accuracy.

Ability to Select Promising Peptides Targeting GPCRs

Identifying peptide candidates with both strong binding affinity and structural stability is crucial for the effective design of GPCR-targeted peptides. To evaluate whether HF-Multistate's confidence scores can aid in this selection process, we assessed their correlation with experimentally measured affinity data from the CXCR4-peptide dataset in PPI-Affinity (Romero-Molina et al., 2022).

We first analyzed the relationship between the peptide average pLDDT and the GPCR-peptide average pAE, as indicated by AF-Multistate and HF-Multistate, in comparison with the binding affinity. According to their physical interpretation in AlphaFold-Multimer (Evans et al., 2021), a higher pLDDT suggests a more structurally plausible, potentially more natural and stable peptide sequence, while a lower pAE indicates greater confidence in binding predictions due to more reliable alignment distances. Although pLDDT and pAE were initially designed

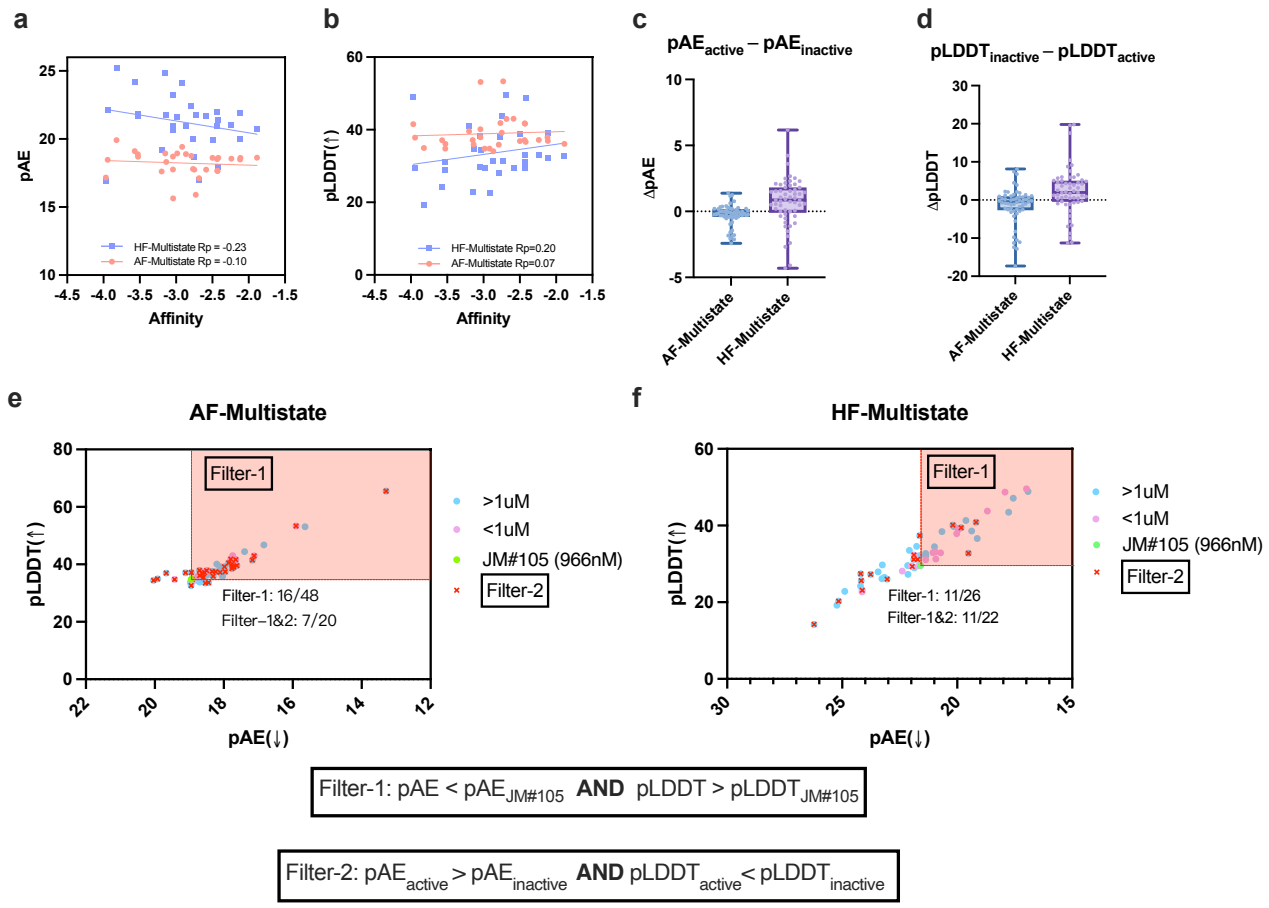

Figure 3. Comparing the screening ability of metrics outputted by AF-Multistate and HF-Multistate. (**a, b**) Pearson correlation analysis of pAE and pLDDT scores with peptide affinity, respectively. The correlation between the metrics of HF-Multistate and experimentally determined affinities is higher than that of AF-Multistate. (**c, d**) Distribution of $\Delta\text{pAE} = \text{pAE}_{\text{active}} - \text{pAE}_{\text{inactive}}$ and $\Delta\text{pLDDT} = \text{pLDDT}_{\text{inactive}} - \text{pLDDT}_{\text{active}}$. $\Delta\text{pAE} > 0$ and $\Delta\text{pLDDT} > 0$ indicate that the peptides act as inhibitors rather than agonists. HF-Multistate effectively distinguishes the functional roles of peptides (whether they are inhibitors or agonists), whereas AF-Multistate does not. **(e, f)** Filter rules for screening peptides with a possible higher affinity than the reference peptide JM#105. The region that satisfies Filter-1 is highlighted in red (Filter-1, containing peptides with confidence scores higher than JM#105). Peptides that do not satisfy Filter-2 are marked with a red cross marker, while peptides that satisfy Filter-2 are represented with other markers, indicating that the model considers them as inhibitors.

to assess structural confidence, our analysis reveals a weak yet consistent correlation between these metrics and GPCR-peptide binding affinity (Figure 3a and Figure 3b). Notably, the correlation between HF-Multistate's predicted metrics and binding affinity is more potent than that of AF-Multistate, suggesting that HF-Multistate provides a more informative structural assessment in this context. This improved correlation indicates its potential to enhance peptide ranking for experimental validation.

To further assess the predictive utility of these multistate models, we examined how their confidence metrics vary when applied to GPCR structures in different activation states. Specifically, we evaluated whether pAE and pLDDT scores can distinguish peptide functionality—such as whether a given peptide acts as an inhibitor—by comparing predictions across active and inactive GPCR states (Figure 3c and Figure 3d). The results indicate that the data points for HF-Multistate predominantly cluster above the zero-axis region of the plot, characterized by $\text{pAE}_{\text{inactive}} < \text{pAE}_{\text{active}}$ and $\text{pLDDT}_{\text{inactive}} > \text{pLDDT}_{\text{active}}$. This suggests that its confidence metrics effectively capture differences in peptide functionality. In contrast, the scores for AF-Multistate do not show significant differences between the various activation states of GPCRs.

The preceding analysis (Figure 3(a-d)) indicates that HF-Multistate's confidence metrics can identify peptides with high affinity and functional relevance for GPCR targeting from multiple perspectives. To further evaluate the combined effectiveness of these predictive capabilities, we applied two filtering rules: Filter 1: excluded candidate peptides with pLDDT or pAE scores inferior to those of the reference peptide (JM#105). Filter 2: Exclude non-inhibitor

peptides, defined as those that do not satisfy $\text{pAE}_{\text{inactive}} < \text{pAE}_{\text{active}}$ or $\text{pLDDT}_{\text{inactive}} > \text{pLDDT}_{\text{active}}$. A comparison of AF-Multistate and HF-Multistate (Figure 3(e-f)) shows that after applying Filter 1, HF-Multistate achieves a hit rate of 11/26 (42%), which is significantly higher than AF-Multistate's 16/48 (33%). After applying both Filter 1 and Filter 2, the hit rate for HF-Multistate increases to 11/22 (50%), while AF-Multistate's hit rate is 7/20 (35%). Notably, AF-Multistate performs only slightly better than the random predictor, which has a hit rate of 17/56 (30%). Here, a hit is defined as a peptide with an affinity below 1 μM, considering that the reference peptide JM#105 has an affinity of 966 nM. These results demonstrate the enhanced capability of HF-Multistate in identifying functionally relevant peptides through a multi-criteria filtering approach.

Validation on APJR

We begin by evaluating our design pipeline using the Apelin Receptor (APJR), a multifunctional G protein-coupled receptor (GPCR) involved in cardiovascular regulation, fluid homeostasis, metabolism, and angiogenesis (O'Carroll et al., 2013). Our objective is to design both agonists and antagonists that target the APJR.

For agonist design, we first employ FoldSeek (Van Kempen et al., 2024), a computational tool for rapid and sensitive structural similarity searches, to identify peptide backbones. We screen for peptides and protein fragments that interact with proteins structurally similar to APJR, serving as candidate scaffolds. Subsequently, a diverse library of 2,400 peptide sequences is generated using a protein inverse folding model (Hsu et al., 2022), which produces peptide sequences to fit the identified backbone structures while accommodating the receptor's binding interface. The designed peptide sequences undergo multiple stages of computational screening (Figure 4a). HF-Multistate is employed to predict the structural conformations of APJR and the peptide candidates, alongside their structural confidence metrics. Based on these evaluations, 70 candidates with pLDDT > 60 and pAE < 10 are selected for further assessment using MMGBSA, a molecular mechanics-based approach that estimates binding free energy by incorporating solvation effects and molecular interactions. From this subset, 11 top-ranking peptides are selected for synthesis and in vitro binding affinity assays. The CHO-K1/AGTRL1/Gα15 cell line is used to express the APJ receptor, and a calcium mobilization assay is performed to quantify receptor activation. A similar strategy is applied for antagonist design.

We first assess whether multiple stages of computational screening effectively identify high-quality peptides. Based on Figures 4a and 4b, all tested peptides exhibit activity toward APJR at concentrations below 100 μM, indicating that HF-Multistate's confidence metrics can effectively identify peptides with potential APJR-binding capability. However, the peptides with the highest affinity, A6 and A11 (highlighted with red diamonds with EC50 values less than 10 nM), do not correspond to the highest pLDDT and pAE scores within the experimental set. This suggests that structural confidence metrics alone are insufficient for accurately ranking binding affinity, highlighting the need to incorporate computational energy-based evaluations, such as MMGBSA, for more precise affinity differentiation. The MMGBSA-derived affinity scores correlate strongly with experimental binding free energy (ΔG_{Exp}) (Figure 4b). Among the three peptides predicted by MMGBSA to have the lowest binding free energies, two agonist peptides (A6 and A11) exhibit EC50 values in the low nanomolar range (<10 nM).

We next examine the experimental validation of the designed peptides, analyzing their dose-response behavior. The corresponding curves for agonists and antagonists are presented in Figures 4c and 4d, respectively.The Relative Light Unit (RLU) indicates the level of receptor activation and response to the peptides. The inhibition ratio measures the percentage of inhibition of the receptor's activity by the peptides. In the agonist design, two peptides demonstrated EC50 values below 10nM, whereas the antagonist design yielded a peptide with an IC50 of 20.3μM.

For comparison, Apelin-13 (Ma et al., 2017), a naturally occurring APJR agonist critical for cardiovascular and metabolic regulation, serves as a reference control for agonist activity (Figure 4c). Although the designed peptides exhibit weaker activity compared to Apelin-13, their sequences differ significantly from Apelin-13, suggesting a potentially distinct binding mode. To gain deeper insights, we constructed a phylogenetic tree comparing several representative peptides with Apelin-13 (Figure 4e). The results demonstrate that the designed peptides exhibit significant sequence divergence from Apelin-13, as well as considerable variation among themselves. Notably, the evolutionary distances between the peptides generally exceed 0.5, highlighting the considerable diversity within our peptide designs.

To gain deeper insights into the interaction patterns, we examined the predicted interaction between Peptide-A6 and APJR, as illustrated in Figure 4f. In comparison with previous studies on AMG3054 (Ma et al., 2017) and

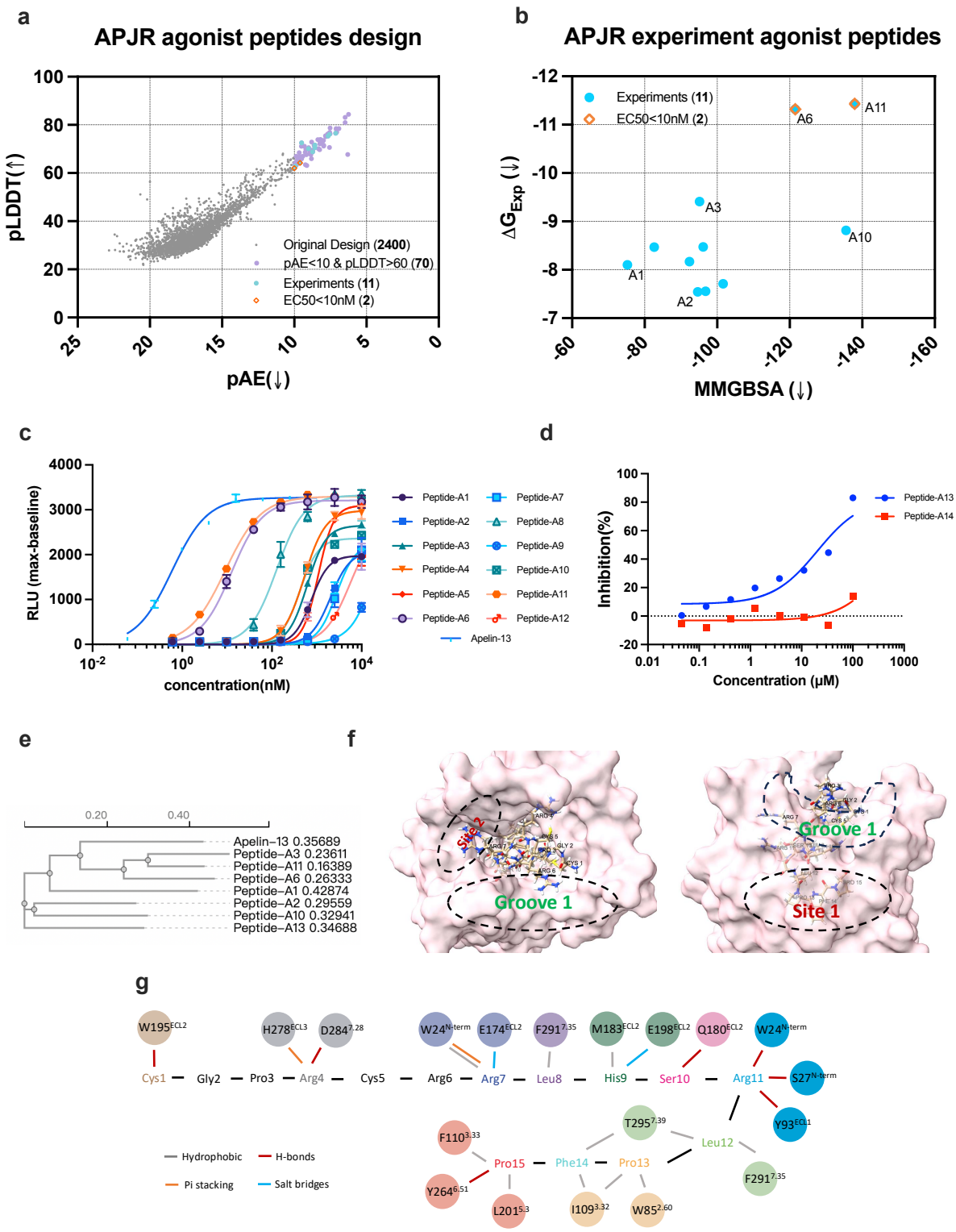

Figure 4. Peptide filtering and analysis for APJR

(a) Multiple stages of computational screening. The distribution of pAE and pLDDT scores for the designed peptides is shown across various stages. **(b)** Experimental binding free energy and MMGBSA scores for the tested APJR agonist peptides. **(c)** Dose-response curves for the tested peptides, showing relative luminescence units (RLU) as a function of peptide concentration (nM). **(d)** Inhibition ratios (%) of APJR activity in response to increasing concentrations of designed APJR antagonist peptides. **(e)** Phylogenetic tree of representative designed peptides alongside Apelin-13. **(f)** Top and lateral views of Peptide-A6 and APJR complex predicted via HelixFold-Multistate. **(g)** Interaction pattern between Peptide-A6 and APJR.

ELA-32 (Yue et al., 2022), Peptide-A6 is found to interact not only with site 1 (F110$^{3.33}$, Y264$^{6.51}$, W85$^{2.60}$, etc.) and

site 2 (W24$^{N\text{-term}}$, D284$^{7.28}$, etc.), but also with groove 1 (E174^{ECL2}, W195^{ECL2}, etc., all in ECL2). Importantly, these residues have been experimentally validated in prior studies, providing additional support for the accuracy of our HF-Multistate predictions in representing the Peptide-A6-APJR complex structure.

Validation on GLP-1R

GLP-1R is a class B GPCR that regulates glucose homeostasis and appetite, making it a key therapeutic target for diabetes and obesity (Knudsen and Lau, 2019; Bucheit et al., 2020; Müller et al., 2022). While numerous agonist peptides, including exenatide, liraglutide, semaglutide, and tirzepatide, have been successfully developed through established approaches, the development of antagonist peptides remains relatively underexplored, despite their potential for treating post-bariatric hypoglycemia (PBH)(Craig et al., 2017). Avexitide (exendin 9-39)(Craig et al., 2021) is one of the few clinically tested antagonists, highlighting both the therapeutic need and the design challenges in this area. This gap provides an opportunity to evaluate our state-specific computational framework for designing more challenging antagonist peptides.

The design pipeline follows a similar approach to that used for APJR. Peptide backbones are first identified using FoldSeek (Van Kempen et al., 2024), followed by the design of antagonist peptide candidates targeting GLP-1R using an inverse folding model (Hsu et al., 2022). The initial design pool consists of approximately 5,000 GLP-1R antagonist candidates, with scores concentrated at the higher end. After applying essential filtering criteria (pLDDT > 85 and pAE < 6.5), around 1,400 peptides remained. Additionally, Filter-2 (introduced in the previous section) is applied to exclude peptides predicted by the model to be functionally inconsistent. Finally, MMGBSA scoring is used to select the top 10 peptides for experimental validation, as shown in Figure 5a. Among these 10 peptides, 4 peptides exhibit inhibitory function, with two of them demonstrating superior affinity compared to the phase-III peptide drug Avexitide (Figure 5b). Moreover, the best antagonist peptide I3 also exhibits the lowest MMGBSA free energy, as shown in Figure 5c.

To explore the novelty of the designed sequences, we compared the designed peptides (I3 and I4) with the sequences of the searched peptide backbones (marked with an asterisk) and Avexitide for similarity. A multiple sequence alignment was performed using MAFFT[1]. Peptide-I3, Peptide-I4, and Avexitide function as antagonists (marked in blue), while SAR425899 (Li et al., 2023), ZP3780 (Hilger et al., 2020), and GLP-1 act as agonists (marked in red). The remaining sequences correspond to unrelated protein segments or peptides identified through the peptide backbone search method (denoted in black). Although the searched peptide backbones (marked with an asterisk) do not include known antagonists, our approach successfully generated novel antagonist peptides, Peptide-I3 and Peptide-I4. Notably, despite their higher sequence similarity to agonists such as GLP-1, both peptides exhibit antagonistic behavior. This finding highlights the accuracy of our structure-based predictions in distinguishing functional roles, even in cases of high sequence similarity.

To better understand how Peptide-I3, despite its sequence similarity to GLP-1, functions as an inhibitor, we aligned the GLP-1–GLP-1R and Peptide-I3–GLP-1R complexes and analyzed their interaction patterns (Figure 5e–j). As shown in Figure 5e, both GLP-1 and Peptide-I3 adopt alpha-helical conformations and occupy the same receptor binding pocket. The receptor adopts an inactive conformation, characterized by an inward displacement of the intracellular end of the TM6 domain (marked in blue) from an active state (marked in red). The differences in the interaction modes of GLP-1 and Peptide-I3 with GLP-1R can be observed in the zoomed-in views, where the common peptide residues (same amino acid type at the exact location) are labeled in black, while the differing peptide residues are marked in red and light blue, respectively. For example, in Figure 5f, the 25-th residue of GLP-1 is Trp(W) with the hydrophobic side chain. In contrast, the 25-th residue of Peptide-I3 is Asp(D) with the negatively charged side chain. As observed, the significant differences are highlighted in Figures 5f, 5h, and 5i. These differences lead to a distinct interaction pattern, as shown in Figure 5j.

Validation on GHSR

The growth hormone secretagogue receptor (GHSR) is a G-protein-coupled receptor that regulates the release of growth hormone and appetite (Kojima et al., 2001). Its endogenous agonist, Ghrelin (Qin et al., 2022), and antagonist, LEAP2 (M'Kadmi et al., 2018), serve as key modulators of its function.

[1] https://www.ebi.ac.uk/jdispatcher/msa/mafft

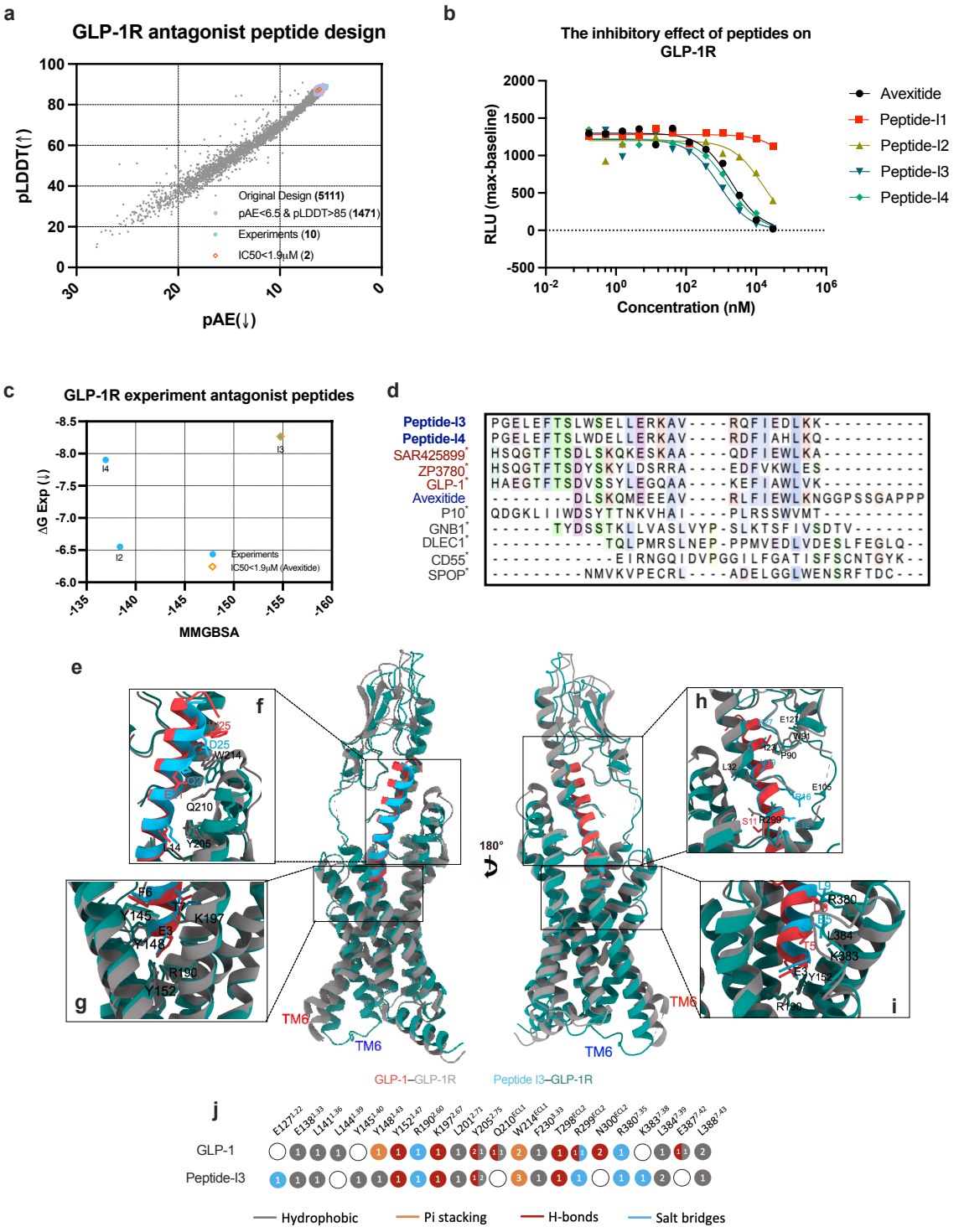

Figure 5. Peptides filtering and analysis for GLP-1R

(a) Multiple stages of computational screening. The distribution of pAE and pLDDT scores for the designed peptides is shown across various stages. **(b)** Inhibitory effects of selected peptides on GLP-1R, comparing their relative fluorescent units against varying concentrations, with Avexitide as a reference. **(c)** Experimental binding free energy and MMGBSA scores for tested GLP-1R antagonist peptides. **(d)** Sequence alignment of Peptide-I3 and Peptide-I4 with Avexitide and top seeds of the peptide backbone (marked with *) used in the design pipeline. Antagonist peptides are indicated in blue, while agonist peptides are shown in red. **(e-i)** GLP-1-GLP-1R and Peptide I3-GLP-1R complexes structure alignment and zoom-in views. The GLP-1 complex is PDB:**6X18**, and the Peptide-I3 complex is predicted by HF-Multistate in an inactive state. **(j)** Comparison of interaction patterns of GLP-1 agonist and Peptide-I3 with the GLP-1 receptor.

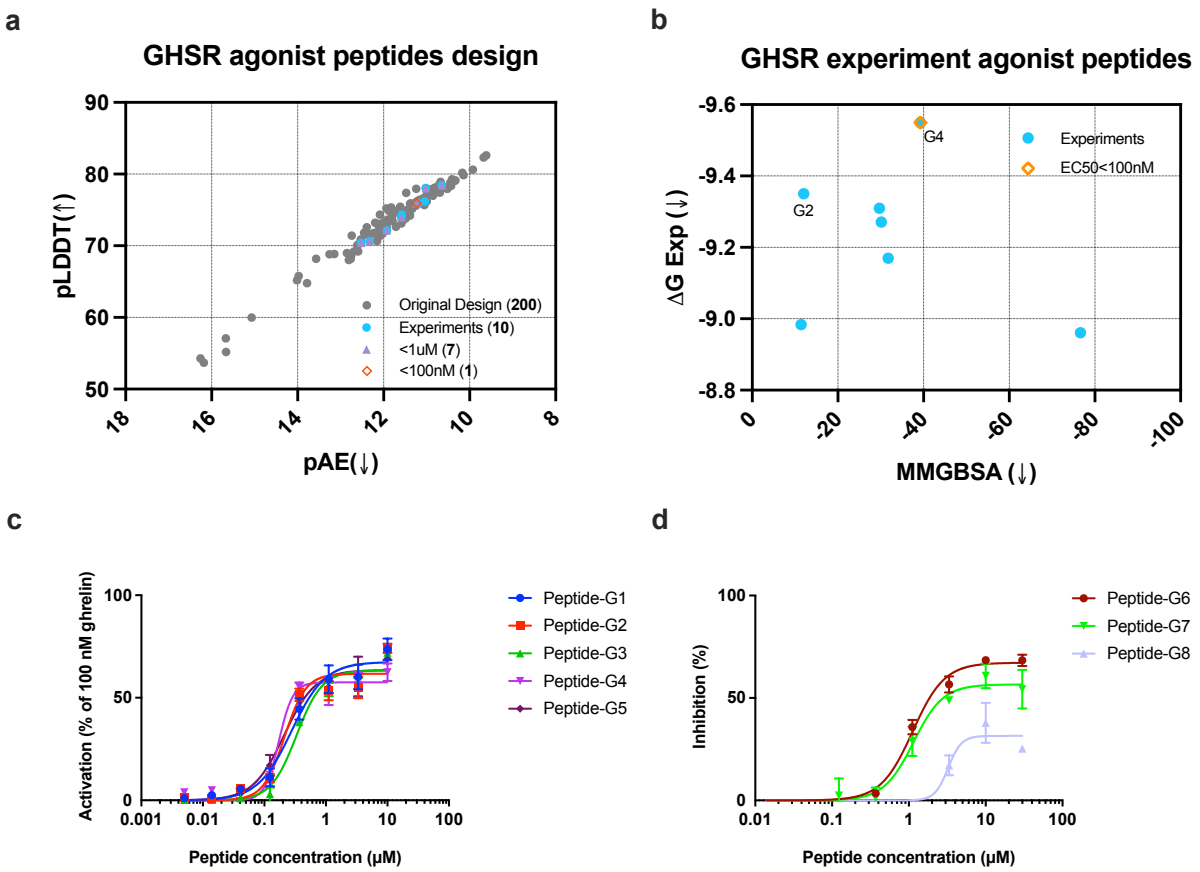

Figure 6. Peptides filtering and analysis for GHSR
(a) Multiple stages of computational screening. The distribution of pAE and pLDDT scores for the designed peptides is shown across various stages. **(b)** Experimental binding free energy and MMGBSA scores for the GHSR agonist peptides tested in the experiments. **(c)** Dose-response curves showing the change in fluorescence intensity ratio (%) as a function of peptide concentration (μM) for various GHSR agonist peptides. **(d)** Inhibition ratios (%) of GHSR activity in response to increasing concentrations of designed GHSR antagonist peptides.

To investigate peptide design strategies that yield well-defined binding interactions, we employed Ghrelin and LEAP2 as seed sequences. Given their established binding modes, we constrained key hotspot residues and utilized ProteinMPNN (Dauparas et al., 2022) to generate a focused library of 200 peptide candidates. Binding affinities were subsequently assessed using HF-Multistate, and candidates with a PLDDT value greater than 70 were selected. We utilize the GHSR state-transition mechanism (Qin et al., 2022) as an additional filtering method. The distance (dWF) WFF cluster indicates peptide activity. A shift toward the active state suggests an agonist, while a shift toward the inactive state implies antagonistic activity (Qin et al., 2022). The remaining candidates were further refined using MMGBSA scoring, and the top 10 peptides were selected for experimental validation (Figure 6a).

For agonist design, Figure 6b illustrates the correlation between MMGBSA-derived affinity scores and experimental binding free energy (ΔG_{Exp}). The majority of tested peptides exhibited EC50 values below 1 μM, with Peptide G4 demonstrating sub-100 nM potency (Figure 6c). This suggests that structure-based design, when combined with computational scoring, can effectively identify high-affinity peptide candidates.

For antagonist design, the inhibition curve in Figure 6d demonstrates that Peptide G6 to G8 exhibited an IC50 in range of 1.0-3.3 μM, effectively disrupting Ghrelin-GHSR interactions. Notably, some peptides derived from the Ghrelin scaffold displayed antagonistic activity, suggesting that HF-Multistate, when specifying GPCR state, can partially capture functional shifts in peptide design. However, attempts to derive inhibitory peptides from the antagonist LEAP2 were unsuccessful, indicating potential limitations in the current approach. Future refinements, such as expanding the design library or enhancing model accuracy, may improve the predictive power of this pipeline.

Discussion

The development of state-specific peptides targeting G protein-coupled receptors (GPCRs) represents a significant advancement in the field of drug discovery and peptide therapeutics. GPCRs, as key mediators of cellular signaling, have long been prime targets for pharmaceutical interventions. Recent successes in GPCR-targeted peptide therapeutics underscore the potential of this approach. For instance, the FDA approval of semaglutide, a GLP-1 receptor agonist peptide for type 2 diabetes and obesity treatment, has demonstrated the clinical efficacy of peptides in modulating GPCR activity (Knudsen and Lau, 2019; Bucheit et al., 2020). Similarly, the development of dasiglucagon, a glucagon receptor agonist peptide for the treatment of severe hypoglycemia, showcases the potential of engineered peptides to improve upon natural ligands in terms of stability and efficacy (Pieber et al., 2021). However, these successes also illuminate the challenges in peptide design, particularly in accounting for the dynamic nature of GPCRs. Traditional peptide design methods often overlook the multiple conformational states of GPCRs, which can significantly impact ligand binding and receptor activation. Our computational pipeline addresses this critical gap by explicitly incorporating the GPCR activation state into the peptide design process. By leveraging diversified seed peptide backbones, inverse folding models for sequence design, and state-specific refolding and scoring for filtering, our approach offers a more nuanced and potentially more effective method for designing GPCR-targeting peptides.

Our state-specific peptide design approach for GPCRs addresses several limitations of existing methods and offers unique advantages. Unlike conventional approaches that rely on natural peptides, phage display, or single-state computational methods, our pipeline explicitly accounts for the dynamic conformational states of GPCRs. This is a significant advancement over recent rational design methods like EvoBind (Bryant and Elofsson, 2022), EvoPlay (Wang et al., 2023), or PepMLM (Chen et al., 2023), which do not consider GPCR state transitions. While approaches like AlphaFold-Multistate (Heo and Feig, 2022) attempt to address GPCR activation states, our experiments revealed its limitations in accurately predicting GPCR-peptide complex structures. Our pipeline overcomes this challenge by combining diversified seed peptides, inverse folding models for sequence generation, and a specifically optimized GPCR-peptide structure prediction model. This integrated approach allows us to design unconstrained, state-specific functional peptides, addressing a gap left by methods like HelixDiff (Xie et al., 2024), which focuses solely on structure-stable helix peptides. However, we acknowledge that the performance difference between agonist and antagonist design highlights an area for future refinement, particularly in designing peptides that must prevent receptor activation.

The success of our state-specific peptide design pipeline for GPCRs opens up exciting avenues for future research and development in the field of peptide therapeutics. While our current work has focused primarily on optimizing binding affinity, future iterations of this approach should aim to simultaneously optimize multiple pharmacological properties. Specifically, enhancing potency and extending half-lives are crucial next steps in developing peptide therapeutics with improved clinical efficacy. This could involve incorporating additional scoring functions or filters that account for factors affecting in vivo stability and receptor activation efficiency. Moreover, the versatility of our approach presents an opportunity to design peptides targeting multiple GPCR targets simultaneously, similar to the multi-target drug tirzepatide. Such multi-target peptides could offer synergistic therapeutic effects and potentially address complex disorders involving multiple GPCR pathways. Another promising direction is the integration of our pipeline with advanced peptide modification techniques, such as cyclization or the incorporation of non-natural amino acids, to further enhance the pharmacokinetic properties of the designed peptides. Furthermore, extending the application of our method to less well-characterized GPCRs could dramatically expand the scope of peptide-based drug discovery. To facilitate this, future work should focus on improving the accuracy of GPCR state prediction for receptors with limited structural data. Lastly, the incorporation of diffusion model techniques to predict all-atom structures directly leads to fewer MSA requirements (Abramson et al., 2024), and peptides may benefit from this. By addressing these future directions, our state-specific peptide design approach has the potential to revolutionize GPCR-targeted therapeutics, leading to the development of more effective and safer peptide drugs with optimized pharmacological profiles.

Methods

A. Data Process

We utilized data from the Propedia v1.0 database (Martins et al., 2021)[2] and GPCRdb (Pándy-Szekeres et al., 2023) (data released before June 30, 2021), comprising over 7,000 entries, to fine-tune HelixFold-Multimer to enhance its capabilities in predicting GPCR-peptide complex structures and improving peptide screening efficiency. To ensure data quality and avoid redundancy, duplicate complexes shared between the two datasets were removed from Propedia during preprocessing, retaining each complex only once.

Our data processing methodology aligns with the workflow used in AlphaFold-Multimer (Evans et al., 2021). For both general protein-peptide and GPCR-peptide complexes, we employed the corresponding template processing pipelines from AlphaFold-Multimer (Evans et al., 2021) and AlphaFold-Multistate (Heo and Feig, 2022). Specifically, for GPCR templates, we selected those that matched both the same class and activation state as the target receptor. This approach ensures that the templates provide a biologically relevant and consistent structural basis for accurate predictions and evaluations.

Data from GPCRdb released after June 30, 2021 (Pándy-Szekeres et al., 2023), filtered for 45 high-quality complexes (30 from class A and 15 from class B), was used to benchmark GPCR-peptide structure prediction across various folding models. It is essential to note that "high-quality complexes" refers to GPCR structures that are intact, enabling evaluation tools like DockQ to accurately align and calculate DockQ scores. The screening evaluation dataset, CXCR4-peptide, was initially collected in PPI-Affinity (Romero-Molina et al., 2022). We compiled the data list and utilized the same multistate data pipeline as mentioned in AlphaFold-Multistate (Heo and Feig, 2022) to process state-specific input features, evaluating and comparing AF-Multistate and our proposed HF-Multistate.

B. Peptide Design Module

To generate backbone seeds, we use the FoldSeek tool (Van Kempen et al., 2024) with default settings to search the Protein Data Bank for crystallized structures similar to the target structure. The search results are then parsed to identify hits that exhibit high contact density in the desired interface area, such as the groove of the GPCR protein's extracellular region. These hits are ranked based on the number of contacts within a continuous segment, and the highest-ranking hit is selected to extract the backbone of the interface segment, which serves as the seed for protein sequence design.

For sequence design, we employ the protein inverse folding model (Hsu et al., 2022), a computational approach that predicts amino acid sequences based on a given three-dimensional structure. In this study, we apply this model to design a diverse set of candidate peptide sequences derived from co-crystal structures of GPCR targets and peptide backbones. These peptide candidates are then evaluated using HF-Multistate to identify the most promising sequences for further investigation.

C. State-Specific Folding Model to Select Promising Peptides

The fine-tuned HelixFold-Multistate model is employed to identify promising peptide candidates by accurately predicting their binding conformations to GPCR targets. All candidate peptides, generated by the peptide design module, are paired with state-specific GPCR targets and undergo structural prediction using this model. The resulting GPCR-peptide complex structures are rigorously assessed to ensure they align with the specified GPCR activation state. Peptides whose predicted structures do not match the target state are systematically filtered out, ensuring that only those with the highest functional relevance are retained for further analysis. In addition, building on the effectiveness of confidence metrics demonstrated by previous studies Wang et al. (2022a); Bennett et al. (2023); Watson et al. (2023); Bryant and Elofsson (2022); Chen et al. (2023); Bhat et al. (2024); Goudy et al. (2023), we incorporate pAE interaction and peptide pLDDT metrics, derived from the folding model, to further refine the selection. A smaller pAE interaction value and a larger peptide pLDDT indicate a better peptide, contributing to a more accurate identification of high-performing candidates. This comprehensive approach increases the reliability of peptide selection for subsequent experimental validation.

[2] http://bioinfo.dcc.ufmg.br/propedia

D. In-Silico Validation

After the initial peptide filtering using HF-Multistate scores, as described in Section C, we utilized MMGBSA to calculate free energy and select candidate peptides with low free energy. For the design of agonist peptides, we applied relaxation similar to AlphaFold-Multimer on the HF-Multistate predicted active complex structure, followed by molecular dynamics (MD) simulations for analysis. In contrast, for the design of antagonist peptides, we utilized the predicted structure of the inactive complex to perform molecular dynamics (MD) simulations.

All MD simulations were conducted using GROMACS (Version 2021) with the Amber03 force field for modeling the interactions within the protein-peptide complex. The system was immersed in a rectangular water box with dimensions approximately 8.5 × 9.5 × 10.5 nm^3, and periodic boundary conditions were applied, resulting in a total system size of about 83,000 atoms comprising a single protein-peptide molecule and around 25,000 water molecules. To neutralize the overall charge, sodium ions were introduced into the system. The system underwent an energy minimization process through steepest descent steps, with a maximum force of 10.0 $kJ{\cdot}mol^{-1}{\cdot}nm^{-1}$ and up to 5,000 steps. Hydrogen-containing bonds were constrained using the LINCS algorithm to enable a time step of 2 fs. Van der Waals interactions were truncated at 1.0 nm, with a gradual switch to zero from 1.0 nm to 1.2 nm for the Lennard-Jones potential. Short-range electrostatic interactions within a cutoff distance of rc = 10 Å were treated as Coulombic interactions. Long-range electrostatic interactions were handled using the particle-mesh Ewald (PME) algorithm. The simulations were performed in the NVT ensemble with a Nośe-Hoover thermostat at 300 K. Pressure coupling was achieved using the Parrinello-Rahman algorithm with a coupling time of τ = 2 ps. Subsequently, the system was equilibrated in the NVT ensemble at 300 K for 100 ps, followed by equilibration in the NPT ensemble at a pressure of 1 bar for an additional 100 ps. The final structure obtained from the NPT equilibration was used as the initial structure for independent molecular dynamics simulations, each lasting 100 ns. Subsequently, the last 500 frames were collected for each system at 2 ps intervals for subsequent MMGBSA calculations. In this research, the MMGBSA calculations utilized one GB models (GB-OBC1). We noted that the choice of interior (solute) dielectric constant could have a significant impact on the predictive accuracy of MMGBSA. Following the MMGBSA benchmark results for the protein-peptide system, interior dielectric constants were employed for these calculations. The exterior (solvent) dielectric constant was maintained at 80.

E. Experimental Validation

Cell lines and eagents. CHO-K1/AGTRL1/Gα15 (#M0025), CHO-K1/GHSR (#M00189) and CHO-K1/GLP1R/Gα15 (#M00451) Stable Cell Lines were purchased from GenScript (NanJing). All peptides including Apelin-13, Ghrelin and Avextide were synthesized by GenScript (NanJing). Calcium5 Assay Kit (#R8186) was purchased from Molecular Device. Probenecid (#P8761) and other chemical reagents were purchased from Sigma (Shanghai).

Calcium mobilization assay. CHO cells stably expressing either the human GHSR receptor or the human hAGTR1 receptor plus the Gα15 protein were digested with 0.25% trypsin and resuspended in cell culture medium and 10,000 cells of CHO-K1/AGTRL1/Gα15, 8,000 cells of CHO-K1/GHSR and 8,000 cells of CHO-K1/GLP1R/Gα15 were transferred respectively to each well of a black Costar 384-well optical bottom plate (Thermo #142761). Each plate was incubated at 37℃, 5% CO2 for 24 h. The culture media was removed from the plates, cells were loaded with Calcium 5 dye in an HBSS-based buffer containing 2.5mM probenecid in a total volume of 50 µL. Cells were incubated at 25℃ for 2h avoiding light, and then stimulated with peptides, Apelin-13 or Ghrelin at various concentrations using a FLIPR Tetra plate-reader (Molecular Device). Agonist-mediated change in fluorescence (ex 488 nm, em 525 nm) was monitored in each well at 1 sec intervals for 160 sec. For antagonist assay, peptides were added at first and the fluorescence was monitored 1 sec intervals for 160 sec, and then Apelin-13, Ghrelin or GLP-1 were added and monitored for another 160 sec. Data were collected using Softmax version 4.8 (MDS Analytical Technologies) and analyzed using Prism software. Nonlinear regression analysis was performed to fit data and obtain maximum response (Emax), EC50, IC50, correlation coefficient (r2), and other parameters. All experiments were performed in duplicate at least 3 times to ensure reproducibility and data are reported as mean ± SEM.

Data Availability

HelixFold-Multistate fine-tuning data: Propedia v1.0 (http://bioinfo.dcc.ufmg.br/propedia/public/download/complex.csv), GPCRdb (https://gpcrdb.org/) (Date cutoff: June 30, 2021).

HelixFold-Multisate folding evaluation dataset: we extracted recent peptide-GPCR PDB data from GPCRdb (see Supplementary Section F), and collected their regions of TM domains from PDBTM (https://pdbtm.unitmp.org/) database for further state-specific analysis.

HelixFold-Multistate score screening evaluation dataset: CXCR4-peptide (Romero-Molina et al., 2022) (https://pubs.acs.org/doi/suppl/10.1021/acs.jproteome.2c00020/suppl_file/pr2c00020_si_001.pdf Table SI-6.1).

Code Availability

FoldSeek (https://github.com/steineggerlab/foldseek), ESM-IF (https://github.com/facebookresearch/esm), AlphaFold-Multistate (https://github.com/huhlim/alphafold-multistate).

Author Contributions

Yang Xue collected and processed the data, as well as fine-tuned and evaluated the HelixFold-Multistate model. Jun Li and Yang Xue implemented the peptide design pipeline and conducted state-specific peptide designs for APJR, GHSR, and GLP-1R. Zhiyuan Chen, Lihang Liu, and Kunrui Zhu supported the base folding model, HelixFold-Multimer. Hong Wang, Jianguo Hu, and Zhi Zheng conducted the web-lab experiments on three GPCR proteins. Jingzhou He, Huanzhang Gong, Xiangqun Li, Xiaonan Zhang, and Xiaomin Fang led the collaborative project, providing resource support and technical guidance.

References

Abramson, J., Adler, J., Dunger, J., Evans, R., Green, T., Pritzel, A., Ronneberger, O., Willmore, L., Ballard, A. J., Bambrick, J., et al. (2024). Accurate structure prediction of biomolecular interactions with alphafold 3. *Nature*, pages 1–3.

Alavi, S. E., Cabot, P. J., and Moyle, P. M. (2019). Glucagon-like peptide-1 receptor agonists and strategies to improve their efficiency. *Molecular pharmaceutics*, 16(6):2278–2295.

Basu, S. and Wallner, B. (2016). Dockq: a quality measure for protein-protein docking models. *PloS one*, 11(8):e0161879.

Bennett, N. R., Coventry, B., Goreshnik, I., Huang, B., Allen, A., Vafeados, D., Peng, Y. P., Dauparas, J., Baek, M., Stewart, L., et al. (2023). Improving de novo protein binder design with deep learning. *Nature Communications*, 14(1):2625.

Bhat, S., Palepu, K., Hong, L., Mao, J., Ye, T., Iyer, R., Zhao, L., Chen, T., Vincoff, S., Watson, R., Wang, T., Srijay, D., Kavirayuni, V. S., Kholina, K., Goel, S., Vure, P., Desphande, A. J., Soderling, S. H., DeLisa, M. P., and Chatterjee, P. (2024). De novo design of peptide binders to conformationally diverse targets with contrastive language modeling. *bioRxiv*. doi: $10.1101/2023.06.26.546591$.

Brown, M. C., Calvete, J. J., Staniszewska, I., Walsh, E. M., Perez-Liz, G., Del Valle, L., Lazarovici, P., and Marcinkiewicz, C. (2007). Vegf-related protein isolated from vipera palestinae venom, promotes angiogenesis. *Growth Factors*, 25(2):108–117.

Bryant, P. and Elofsson, A. (2022). Evobind: in silico directed evolution of peptide binders with alphafold. *bioRxiv*, pages 2022–07.

Bucheit, J. D., Pamulapati, L. G., Carter, N., Malloy, K., Dixon, D. L., and Sisson, E. M. (2020). Oral semaglutide: a review of the first oral glucagon-like peptide 1 receptor agonist. *Diabetes technology & therapeutics*, 22(1):10–18.

Chang, L., Mondal, A., and Perez, A. (2022). Towards rational computational peptide design. *Frontiers in Bioinformatics*, 2: 1046493.

Chen, T., Pertsemlidis, S., Watson, R., Kavirayuni, V. S., Hsu, A., Vure, P., Pulugurta, R., Vincoff, S., Hong, L., Wang, T., et al. (2023). Pepmlm: Target sequence-conditioned generation of peptide binders via masked language modeling. *ArXiv*.

Craig, C. M., Liu, L.-F., Deacon, C. F., Holst, J. J., and McLaughlin, T. L. (2017). Critical role for glp-1 in symptomatic post-bariatric hypoglycaemia. *Diabetologia*, 60:531–540.

Craig, C. M., Lawler, H. M., Lee, C. J. E., Tan, M., Davis, D. B., Tong, J., Glodowski, M., Rogowitz, E., Karaman, R., McLaughlin, T. L., et al. (2021). Prevent: a randomized, placebo-controlled crossover trial of avexitide for treatment of postbariatric hypoglycemia. *The Journal of Clinical Endocrinology & Metabolism*, 106(8):e3235–e3248.

Dauparas, J., Anishchenko, I., Bennett, N., Bai, H., Ragotte, R. J., Milles, L. F., Wicky, B. I., Courbet, A., de Haas, R. J., Bethel, N., et al. (2022). Robust deep learning–based protein sequence design using proteinmpnn. *Science*, 378(6615):49–56.

Davenport, A. P., Scully, C. C., de Graaf, C., Brown, A. J., and Maguire, J. J. (2020). Advances in therapeutic peptides targeting g protein-coupled receptors. *Nature Reviews Drug Discovery*, 19(6):389–413.

Evans, R., O'Neill, M., Pritzel, A., Antropova, N., Senior, A., Green, T., Žídek, A., Bates, R., Blackwell, S., Yim, J., et al. (2021). Protein complex prediction with alphafold-multimer. *biorxiv*, pages 2021–10.

Fang, X., Gao, J., Hu, J., Liu, L., Xue, Y., Zhang, X., and Zhu, K. (2024). Helixfold-multimer: Elevating protein complex structure prediction to new heights. *arXiv preprint arXiv:2404.10260*.

Goudy, O. J., Nallathambi, A., Kinjo, T., Randolph, N. Z., and Kuhlman, B. (2023). In silico evolution of autoinhibitory domains for a pd-l1 antagonist using deep learning models. *Proceedings of the National Academy of Sciences*, 120(49):e2307371120.

Hauser, A. S., Kooistra, A. J., Munk, C., Heydenreich, F. M., Veprintsev, D. B., Bouvier, M., Babu, M. M., and Gloriam, D. E. (2021). Gpcr activation mechanisms across classes and macro/microscales. *Nature structural & molecular biology*, 28(11): 879–888.

Heo, L. and Feig, M. (2022). Multi-state modeling of g-protein coupled receptors at experimental accuracy. *Proteins: Structure, Function, and Bioinformatics*, 90(11):1873–1885.

Hilger, D., Kumar, K. K., Hu, H., Pedersen, M. F., O'Brien, E. S., Giehm, L., Jennings, C., Eskici, G., Inoue, A., Lerch, M., et al. (2020). Structural insights into differences in g protein activation by family a and family b gpcrs. *Science*, 369(6503):eaba3373.

Hill, T. A., Shepherd, N. E., Diness, F., and Fairlie, D. P. (2014). Constraining cyclic peptides to mimic protein structure motifs. *Angewandte Chemie International Edition*, 53(48):13020–13041.

Hsu, C., Verkuil, R., Liu, J., Lin, Z., Hie, B., Sercu, T., Lerer, A., and Rives, A. Learning inverse folding from millions of predicted structures. In *International conference on machine learning*, pages 8946–8970. PMLR, (2022).

Knudsen, L. B. and Lau, J. (2019). The discovery and development of liraglutide and semaglutide. *Frontiers in endocrinology*, 10:155.

Kojima, M., Hosoda, H., Matsuo, H., and Kangawa, K. (2001). Ghrelin: discovery of the natural endogenous ligand for the growth hormone secretagogue receptor. *Trends in Endocrinology & Metabolism*, 12(3):118–122.

Li, Q., Vlachos, E. N., and Bryant, P. (2024). Design of linear and cyclic peptide binders of different lengths only from a protein target sequence. *bioRxiv*, pages 2024–06.

Li, Y., Zhou, Q., Dai, A., Zhao, F., Chang, R., Ying, T., Wu, B., Yang, D., Wang, M.-W., and Cong, Z. (2023). Structural analysis of the dual agonism at glp-1r and gcgr. *Proceedings of the National Academy of Sciences*, 120(33):e2303696120.

Ma, Y., Yue, Y., Ma, Y., Zhang, Q., Zhou, Q., Song, Y., Shen, Y., Li, X., Ma, X., Li, C., et al. (2017). Structural basis for apelin control of the human apelin receptor. *Structure*, 25(6):858–866.

Martins, P. M., Santos, L. H., Mariano, D., Queiroz, F. C., Bastos, L. L., Gomes, I. d. S., Fischer, P. H., Rocha, R. E., Silveira, S. A., de Lima, L. H., et al. (2021). Propedia: a database for protein–peptide identification based on a hybrid clustering algorithm. *BMC bioinformatics*, 22:1–20.

Matsubayashi, Y. and Sakagami, Y. (2006). Peptide hormones in plants. *Annu. Rev. Plant Biol.*, 57:649–674.

Müller, T. D., Blüher, M., Tschöp, M. H., and DiMarchi, R. D. (2022). Anti-obesity drug discovery: advances and challenges. *Nature Reviews Drug Discovery*, 21(3):201–223.

Mygind, P. H., Fischer, R. L., Schnorr, K. M., Hansen, M. T., Sönksen, C. P., Ludvigsen, S., Raventós, D., Buskov, S., Christensen, B., De Maria, L., et al. (2005). Plectasin is a peptide antibiotic with therapeutic potential from a saprophytic fungus. *Nature*, 437(7061):975–980.

M'Kadmi, C., Cabral, A., Barrile, F., Giribaldi, J., Cantel, S., Damian, M., Mary, S., Denoyelle, S., Dutertre, S., Péraldi-Roux, S., et al. (2018). N-terminal liver-expressed antimicrobial peptide 2 (leap2) region exhibits inverse agonist activity toward the ghrelin receptor. *Journal of Medicinal Chemistry*, 62(2):965–973.

Nevola, L. and Giralt, E. (2015). Modulating protein–protein interactions: the potential of peptides. *Chemical Communications*, 51(16):3302–3315.

Omidfar, K. and Daneshpour, M. (2015). Advances in phage display technology for drug discovery. *Expert opinion on drug discovery*, 10(6):651–669.

O'Carroll, A.-M., Lolait, S. J., Harris, L. E., and Pope, G. R. (2013). The apelin receptor apj: journey from an orphan to a multifaceted regulator of homeostasis. *J Endocrinol*, 219(1):R13–35.

Pacesa, M., Nickel, L., Schmidt, J., Pyatova, E., Schellhaas, C., Kissling, L., Alcaraz-Serna, A., Cho, Y., Ghamary, K. H., Vinue, L., et al. (2024). Bindcraft: one-shot design of functional protein binders. *bioRxiv*, pages 2024–09.

Pándy-Szekeres, G., Caroli, J., Mamyrbekov, A., Kermani, A. A., Keserű, G. M., Kooistra, A. J., and Gloriam, D. E. (2023). Gpcrdb in 2023: state-specific structure models using alphafold2 and new ligand resources. *Nucleic acids research*, 51(D1): D395–D402.

Pieber, T. R., Aronson, R., Hövelmann, U., Willard, J., Plum-Mörschel, L., Knudsen, K. M., Bandak, B., and Tehranchi, R. (2021). Dasiglucagon—a next-generation glucagon analog for rapid and effective treatment of severe hypoglycemia: results of phase 3 randomized double-blind clinical trial. *Diabetes Care*, 44(6):1361–1367.

Pokuri, V. K., Fong, M. K., and Iyer, R. (2016). Octreotide and lanreotide in gastroenteropancreatic neuroendocrine tumors. *Current oncology reports*, 18:1–9.

Qin, J., Cai, Y., Xu, Z., Ming, Q., Ji, S.-Y., Wu, C., Zhang, H., Mao, C., Shen, D.-D., Hirata, K., et al. (2022). Molecular mechanism of agonism and inverse agonism in ghrelin receptor. *Nature Communications*, 13(1):300.

Romero-Molina, S., Ruiz-Blanco, Y. B., Mieres-Perez, J., Harms, M., Munch, J., Ehrmann, M., and Sanchez-Garcia, E. (2022). Ppi-affinity: A web tool for the prediction and optimization of protein–peptide and protein–protein binding affinity. *Journal of proteome research*, 21(8):1829–1841.

Santos, R., Ursu, O., Gaulton, A., Bento, A. P., Donadi, R. S., Bologa, C. G., Karlsson, A., Al-Lazikani, B., Hersey, A., Oprea, T. I., et al. (2017). A comprehensive map of molecular drug targets. *Nature reviews Drug discovery*, 16(1):19–34.

Silver, D., Huang, A., Maddison, C. J., Guez, A., Sifre, L., Van Den Driessche, G., Schrittwieser, J., Antonoglou, I., Panneershelvam, V., Lanctot, M., et al. (2016). Mastering the game of go with deep neural networks and tree search. *nature*, 529(7587):484–489.

Toivanen, P. I., Nieminen, T., Laakkonen, J. P., Heikura, T., Kaikkonen, M. U., and Ylä-Herttuala, S. (2017). Snake venom vegf vammin induces a highly efficient angiogenic response in skeletal muscle via vegfr-2/nrp specific signaling. *Scientific reports*, 7(1):5525.

Van Kempen, M., Kim, S. S., Tumescheit, C., Mirdita, M., Lee, J., Gilchrist, C. L., Söding, J., and Steinegger, M. (2024). Fast and accurate protein structure search with foldseek. *Nature biotechnology*, 42(2):243–246.

Vázquez Torres, S., Leung, P. J., Venkatesh, P., Lutz, I. D., Hink, F., Huynh, H.-H., Becker, J., Yeh, A. H.-W., Juergens, D., Bennett, N. R., et al. (2024). De novo design of high-affinity binders of bioactive helical peptides. *Nature*, 626(7998):435–442.

Wang, J., Lisanza, S., Juergens, D., Tischer, D., Watson, J. L., Castro, K. M., Ragotte, R., Saragovi, A., Milles, L. F., Baek, M., et al. (2022). Scaffolding protein functional sites using deep learning. *Science*, 377(6604):387–394.

Wang, L., Wang, N., Zhang, W., Cheng, X., Yan, Z., Shao, G., Wang, X., Wang, R., and Fu, C. (2022). Therapeutic peptides: current applications and future directions. *Signal Transduction and Targeted Therapy*, 7(1):48.

Wang, Y., Tang, H., Huang, L., Pan, L., Yang, L., Yang, H., Mu, F., and Yang, M. (2023). Self-play reinforcement learning guides protein engineering. *Nature Machine Intelligence*, 5(8):845–860.

Watson, J. L., Juergens, D., Bennett, N. R., Trippe, B. L., Yim, J., Eisenach, H. E., Ahern, W., Borst, A. J., Ragotte, R. J., Milles, L. F., et al. (2023). De novo design of protein structure and function with rfdiffusion. *Nature*, 620(7976):1089–1100.

Weiss, D. R., Karpiak, J., Huang, X.-P., Sassano, M. F., Lyu, J., Roth, B. L., and Shoichet, B. K. (2018). Selectivity challenges in docking screens for gpcr targets and antitargets. *Journal of medicinal chemistry*, 61(15):6830–6845.

Wilson, A. C., Vadakkadath Meethal, S., Bowen, R. L., and Atwood, C. S. (2007). Leuprolide acetate: a drug of diverse clinical applications. *Expert opinion on investigational drugs*, 16(11):1851–1863.

Xie, X., Valiente, P. A., Kim, J., and Kim, P. M. (2024). Helixdiff, a score-based diffusion model for generating all-atom α-helical structures. *ACS Central Science*.

Yamazaki, Y., Matsunaga, Y., Tokunaga, Y., Obayashi, S., Saito, M., and Morita, T. (2009). Snake venom vascular endothelial growth factors (vegf-fs) exclusively vary their structures and functions among species. *Journal of biological chemistry*, 284(15): 9885–9891.

Yue, Y., Liu, L., Wu, L.-J., Wu, Y., Wang, L., Li, F., Liu, J., Han, G.-W., Chen, B., Lin, X., et al. (2022). Structural insight into apelin receptor-g protein stoichiometry. *Nature structural & molecular biology*, 29(7):688–697.

Zambaldi, V., La, D., Chu, A. E., Patani, H., Danson, A. E., Kwan, T. O., Frerix, T., Schneider, R. G., Saxton, D., Thillaisundaram, A., et al. (2024). De novo design of high-affinity protein binders with alphaproteo. *arXiv preprint arXiv:2409.08022*.

Supplementary Information

F. HelixFold-Multistate folding evaluation data

Recent peptide-GPCR class A PDBs. 7SK7, 7VFX, 7SK4, 7SK5, 7F6G, 7W0P, 7Y67, 7XA3, 7YJ4, 7SK3, 7SK6, 7YKD, 7XWO, 7SK8, 7Y66, 7XNA, 7YON, 7Y1F, 7Y64, 8HK5, 8HK2, 8F7Q, 8H0Q, 8F7W, 8DWC, 8F7X, 8DWG, 8H0P, 8F7R, 8IA8.

Recent peptide-GPCR class B PDBs. 7VVN, 7VVL, 7VVK, 7VVJ, 7VVM, 8FLU, 8F0J, 8F0K, 8FLR, 8HA0, 8F2B, 8HAF, 8HAO, 8F2A, 8FLQ.

G. HelixFold-Multistate folding evaluation

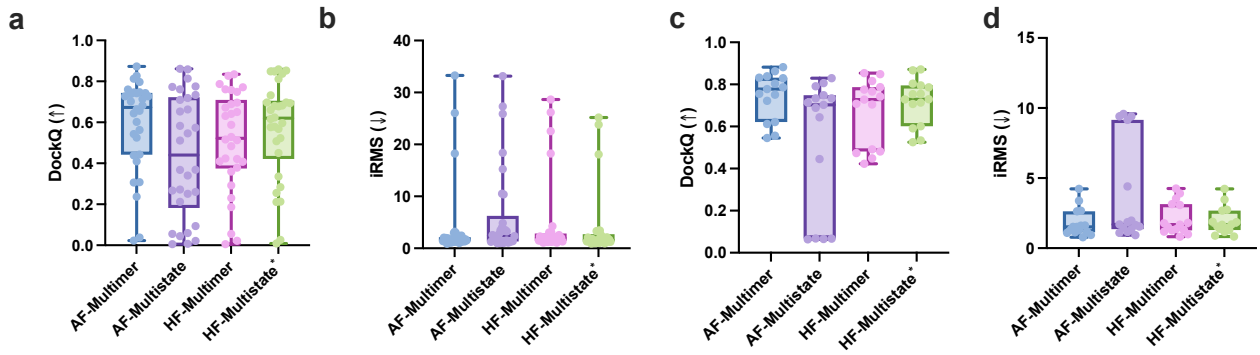

Figure S1. Comparing activation state prediction performance for GPCR class A and B using DockQ and iRMS metrics. (a) and **(b)** correspond to GPCR Class A, while **(c)** and **(d)** pertain to GPCR Class B.

H. GHSR Molecular Simulation Analysis

As a type of GPCR protein, GHSR possesses not only its specific WFF cluster but also general state-specific features, such as significant transformations of the TM6 domain. We have listed all of these features below:

- dw: width of WFF cluster, specifically the distance between W$276^{6.48}$ and F$312^{7.42}$.
- TM6 RMSD: TM6 RMSD against active (RMSD$_a$) and inactive states (RMSD$_i$).
- d: the distance of intracellular end of TM6 towards active (d_a) and inactive (d_i) states.
- θ: the swing angle of intracellular end of TM6 from active (θ_a) and inactive (θ_i) states.

Theoretically, if the state of GHSR state transition happends during simulation, it indicates the predicted GHSR-peptide structure is unstable, and the peptide either has reverse functionality or doesn't have affinity. Before conducting such simulation, we first analysis the influence of membrane on these measurements. As a results in Figure S4, the membrane does not have effect on the change direction, but on the amplitude of the change. Considering the large computation resources increase when simulate with membrane, we remove it then do the simulation for 10ns for each peptide design. Figure S5 compares width of WFF cluster trajectories of our designed agonist and antagonist peptides.

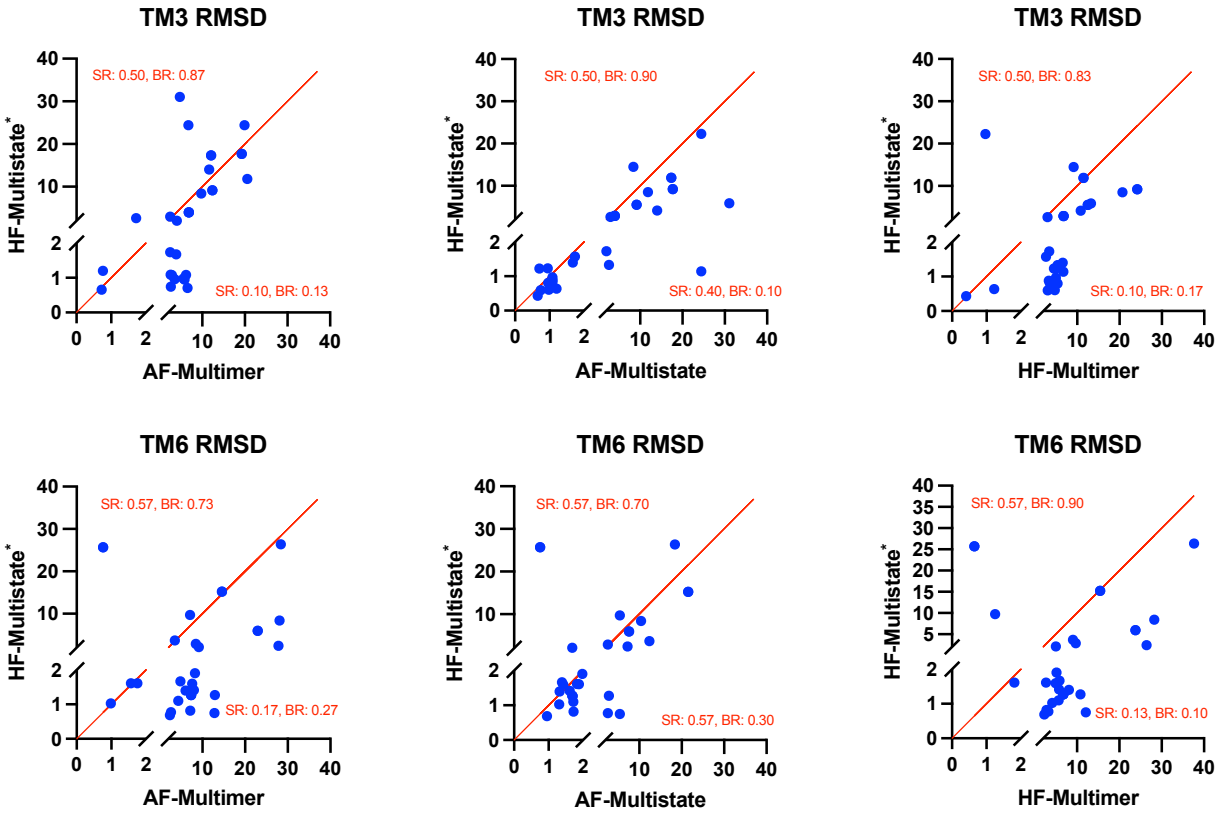

Figure S2. Comparing activation state prediction performance for GPCR class A on TM3 and TM6 domains. For GPCR class A proteins, their activation states are mainly determined by TM3 and TM6 domains. The corresponding RMSD metrics reflect that our proposed HF-Multistate model outperforms baselines in terms of SR (success rate) and BR (beat rate).

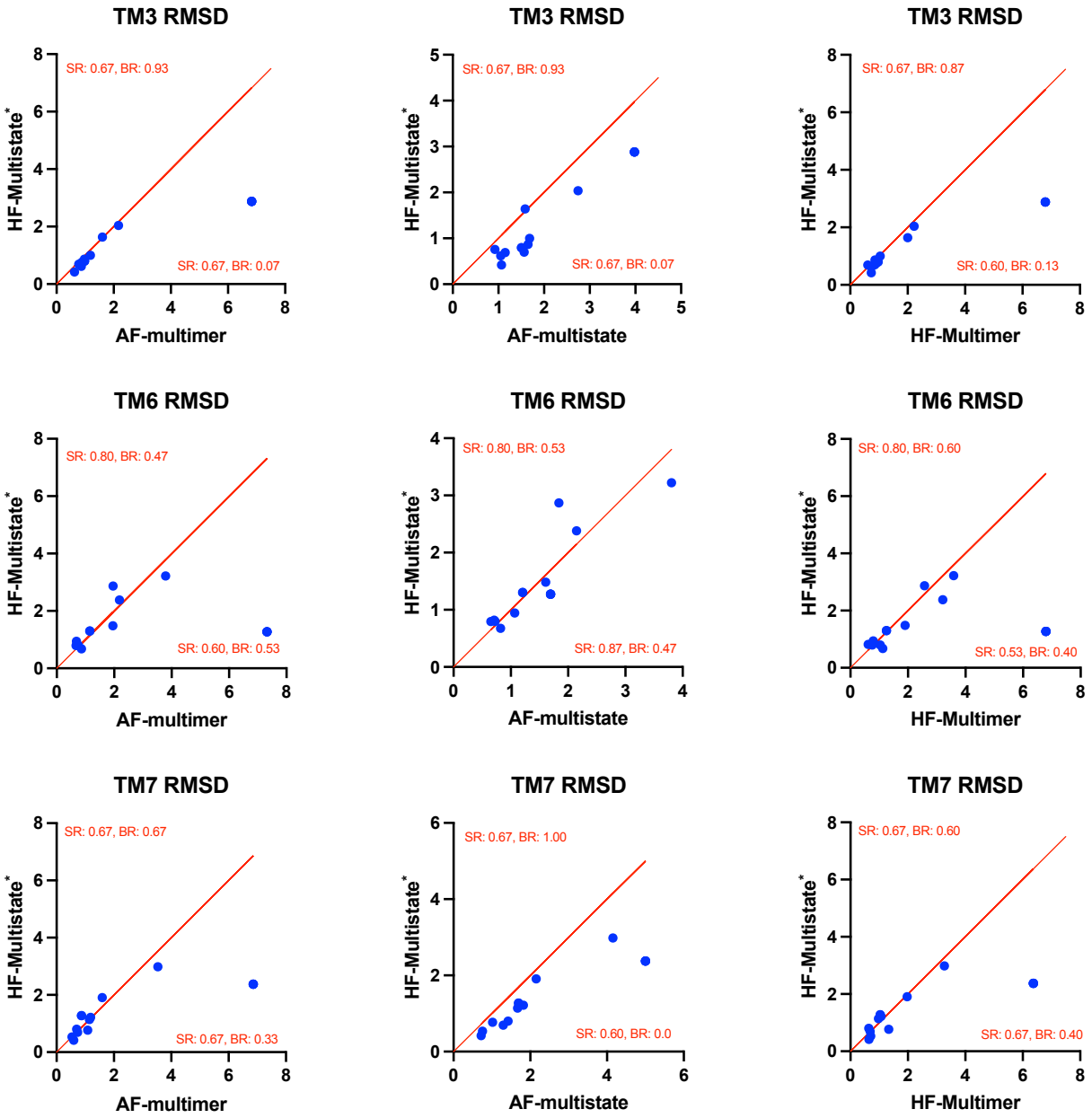

Figure S3. Comparing activation state prediction performance for GPCR class B on TM3, TM6 and TM7 domains. For GPCR class B proteins, their activation states are mainly determined by TM3, TM6 and TM7 domains. Unlike GPCR class A (Figure S2), there is less PDB data for class B, and the margin between HF-Multistate and baseline models is smaller.

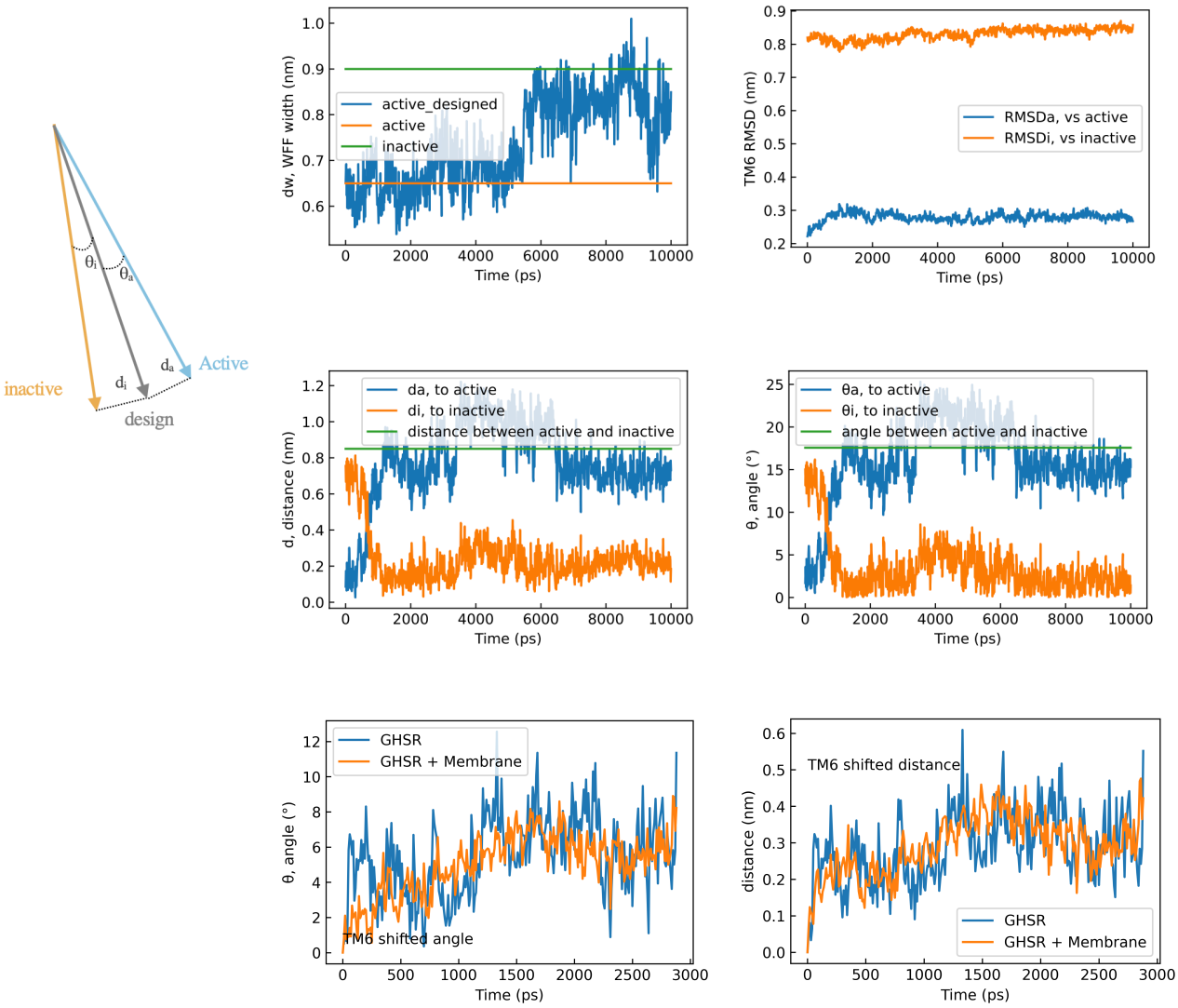

Figure S4. GHSR MD trajectories of state-specific features.

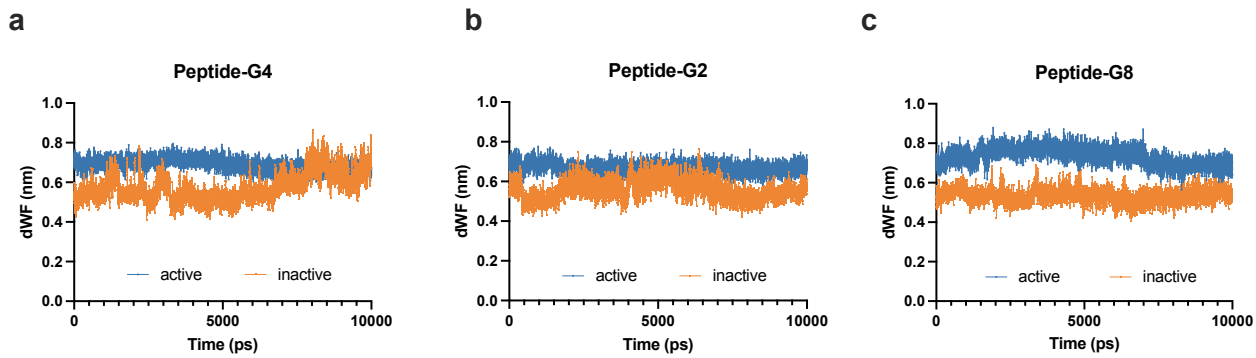

Figure S5. GHSR WFF trajectories of agonist and antagonist peptides.
Simulation trajectory of the dWF (distance between $W276^{6.48}$ and $F312^{7.42}$) for agonist Peptide-G4 **(a)**, agonist Peptide-G2 **(b)**, and antagonist Peptide-G8 **(c)** over a 10-ns simulation for both active and inactive conformations.